Efficient *ab initio* Migdal-Eliashberg calculation considering the retardation effect in phonon-mediated superconductors

Tianchun Wang [1,*], Takuya Nomoto [1], Yusuke Nomura [2], Hiroshi Shinaoka [3], Junya Otsuki [4], Takashi Koretsune [5], and Ryotaro Arita [1,2]

[1]*Department of Applied Physics, The University of Tokyo, 7-3-1 Hongo, Bunkyo-ku, Tokyo 113-8656, Japan*
[2]*RIKEN Center for Emergent Matter Science, 2-1 Hirosawa, Wako, Saitama 351-0198, Japan*
[3]*Department of Physics, Saitama University, Sakura, Saitama 338-8570, Japan*
[4]*Research Institute for Interdisciplinary Science, Okayama University, Okayama 700-8530, Japan*
[5]*Department of Physics, Tohoku University, Miyagi 980-8578, Japan*

We formulate an efficient scheme to perform a Migdal-Eliashberg calculation considering the retardation effect from first principles. While the conventional approach requires a huge number of Matsubara frequencies, we show that the intermediate representation of the Green's function [H. Shinaoka *et al.*, Phys. Rev. B **96**, 035147 (2017)] dramatically reduces the numerical cost to solve the linearized gap equation. Without introducing any empirical parameter, we obtain a superconducting transition temperature of elemental Nb ($\sim$10 K), which is consistent with experiment. The present result indicates that our approach has a superior performance for many superconductors for which T_c is lower than $O(10)$ K.

I. INTRODUCTION

Ab initio calculation of the superconducting transition temperature (T_c) has been an intriguing challenge in computational condensed-matter physics [1,2]. Based on the experimental phonon spectrum of elemental Nb and the Migdal-Eliashberg theory, McMillan [3] and Allen and Dynes [4] derived a formula to calculate T_c of phonon-mediated superconductors. While the McMillan-Allen-Dynes formula has been widely used to estimate T_c of a variety of superconductors [1], one crucial problem is that it contains the pseudo-Coulomb interaction parameter μ^* [5]. Although there were some efforts made to improve the derivation of μ^* [6,7], and to calculate it from first principles [8], μ^* is usually treated as an adjustable parameter [2,9]. Thus the McMillan-Allen-Dynes formula cannot be used for predicting T_c of unknown superconductors.

On the other hand, it has been well known that the numerical cost of *ab initio* momentum-dependent Migdal-Eliashberg calculation is formidably high [10,11]. Especially when T_c is relatively low, the retardation effect [5] becomes more and more difficult to treat numerically [2]. While the typical energy scale of the dynamical structure of the electron-phonon interaction is just 10 meV, that of the screened Coulomb interaction is as large as the bandwidth ($W \sim 10$ eV). Thus in the scheme based on the Matsubara Green's function, we need to introduce an extremely large number of Matsubara frequencies (N_M) to describe the frequency dependence of the effective interaction between electrons accurately. In many cases, N_M should be as large as W/T to obtain a well-

converged solution, where T is the temperature. Therefore, *ab initio* Migdal-Eliashberg calculation requires a considerably large amount of memory and computation time, and it has been performed only for hydride superconductors having $T_c \sim 200$ K under high pressures [2,12,13].

In addition to the approach based on the Migdal-Eliashberg theory, there is another approach based on an extension of density functional theory, namely the so-called superconducting density functional theory (SCDFT) [14–18]. In SCDFT, the gap equation consists of static quantities that do not depend on frequency, so that we can solve the gap equation in SCDFT much more efficiently than that in the Migdal-Eliashberg theory. Indeed, SCDFT calculations have been performed for many conventional superconductors [2,16–22].

In Ref. [16], the kernel of the SCDFT gap equation was constructed based on the Kohn-Sham perturbation theory. There, to describe the mass enhancement effect due to the electron-phonon coupling, the bare Green's function rather than the fully dressed Green's function was employed. Therefore, the treatment of the mass enhancement effect in Ref. [16] is not self-consistent. In fact, there is no guarantee that this treatment always works successfully. When it does not work, it is a highly nontrivial challenge to derive a better exchange-correlation functional [23]. On the other hand, in the Migdal-Eliashberg theory, we know what kind of diagrams are considered to dress the Green's function, and it is easier to improve the calculation systematically. Thus, the development of an efficient scheme to perform the Migdal-Eliashberg calculation based on the fully dressed Green's function is highly desired.

Recently, a method that can solve the long-standing problem of a large number of Matsubara frequencies was developed [24]. This method is based on a compact and efficient

*tiachun.wang@riken.jp

134503-1

representation [which we call an intermediate-representation (IR)] of the Green's functions proposed by two of the present authors and their collaborators [24–28]. The IR basis not only provides us with a compact representation of the Green's function, but it also enables us to perform efficient many-body calculations with the Green's functions. The number of basis functions (the IR basis) required to store and reconstruct the Green's functions both in imaginary-time space and Matsubara-frequency space is much smaller than that of the conventional Legendre polynomials. There, it has been shown that the conventional uniform Matsubara-frequency grid can be replaced by a series of sparse sampling points to describe the frequency dependence of the IR basis and hence Green's functions [28]. Using the sparse sampling method, we can reconstruct the Matsubara Green's function with only about 100 points on the frequency grid, and we can transform efficiently the imaginary-time Green's function to the Matsubara Green's function and vice versa. It is worth noting that there have been studies on the acceleration to obtain self-consistent field solutions [29]. A recent study has also been proposed [30] to perform Migdal-Eliashberg calculations with improved numerical performance, in which the high-energy part and the low-energy part of the calculations are treated separately. It should be noted that the present approach based on the IR basis is a direct numerical calculation without any approximations.

In this paper, we formulate a scheme to perform *ab initio* Migdal-Eliashberg calculation with the IR basis. We find that we can solve the anisotropic (momentum-dependent) gap equation very efficiently. We show the results for two different superconductors: one is elemental Nb with $T_c \sim 10$ K, and the other is LaH$_{10}$ under 250 GPa with $T_c \sim 200$ K [13]. With these benchmark calculations, we demonstrate that our approach has a superior performance, especially when T_c is lower than $O(10)$ K.

II. METHOD

A. Eliashberg equation

In the framework of the Migdal-Eliashberg theory [1,2,31,32], we calculate the superconducting T_c by solving the gap equation

$$\Delta_m(\boldsymbol{k}, i\omega_n)$$
$$= -\frac{T}{N_{\boldsymbol{k}}} \sum_{m'} \sum_{\boldsymbol{k}',i\omega_{n'}} \mathcal{K}_{mm'}(\boldsymbol{k}-\boldsymbol{k}', i\omega_n - i\omega_{n'}) F_{m'}(\boldsymbol{k}', i\omega_{n'}),$$
$$(1)$$

where Δ_m is the superconducting gap function, $\mathcal{K}_{mm'}$ is a pairing-interaction kernel, and $F_{m'}$ is the anomalous Green's function, which are functions of the electron momenta $\boldsymbol{k}, \boldsymbol{k}'$, Matsubara frequencies $\omega_n, \omega_{n'}$, and band indices m, m'. $N_{\boldsymbol{k}}$ denotes the total number of $\boldsymbol{k}$-points. T_c is the highest temperature T at which Δ_m is finite.

In the following calculations, we solve the linearized gap equation to calculate T_c, where the anomalous Green's function can be written as

$$F_m(\boldsymbol{k}, i\omega_n) = |G_m(\boldsymbol{k}, i\omega_n)|^2 \Delta_m(\boldsymbol{k}, i\omega_n), \quad (2)$$

where $G_m(\boldsymbol{k}, i\omega_n)$ is the electron Green's function. The kernel $\mathcal{K}_{mm'}$ consists of the contributions from the attractive interaction due to electron-phonon coupling and the repulsive screened Coulomb interaction as

$$\mathcal{K}_{mm'} = \mathcal{K}_{mm'}^{\text{el}-\text{ph}} + \mathcal{K}_{mm'}^{\text{C}}. \quad (3)$$

Let us first focus on the first term and leave the treatment of the second term in Sec. II B. Considering the electron-phonon interaction as a scattering process of electrons from momentum $\boldsymbol{k}$ to $\boldsymbol{k}-\boldsymbol{q}$ mediated by a phonon with a momentum $\boldsymbol{q}$, we can write $\mathcal{K}_{mm'}^{\text{el}-\text{ph}}$ as

$$\mathcal{K}_{mm'}^{\text{el}-\text{ph}}(\boldsymbol{q}, i\omega_\nu) = \sum_\lambda \left| \mathrm{g}_\lambda^{mm'}(\boldsymbol{q}) \right|^2 D_\lambda(\boldsymbol{q}, i\omega_\nu), \quad (4)$$

where λ and ω_ν are the phonon's mode index and the Matsubara frequency of bosons, respectively. Here we assume that the electron-phonon interaction matrix element $\mathrm{g}_\lambda^{m\boldsymbol{k},m'\boldsymbol{k}-\boldsymbol{q}}$ does not depend on $\boldsymbol{k}$ significantly, thus we take an average over $\boldsymbol{k}$ around the Fermi level, and we use a $\boldsymbol{k}$-average one $\mathrm{g}_\lambda^{mm'}(\boldsymbol{q})$ in Eq. (4). For conventional superconductors, ignoring the $\boldsymbol{k}$-dependence of $\mathrm{g}_\lambda^{m\boldsymbol{k},m'\boldsymbol{k}-\boldsymbol{q}}$ could be a good approximation, since the gap function is almost isotropic. This approximation was successful in the recent studies of sulfur hydrides [12], and we think it could be good approximation for our following calculations. For a detailed discussion on this $\boldsymbol{k}$-average approximation, we refer the reader to the Appendix. The phonon Green's function $D_\lambda(\boldsymbol{q}, i\omega_\nu)$ is given as

$$D_\lambda(\boldsymbol{q}, i\omega_\nu) = -\frac{2\omega_{\boldsymbol{q}\lambda}}{\omega_\nu^2 + \omega_{\boldsymbol{q}\lambda}^2}, \quad (5)$$

where $\omega_{\boldsymbol{q}\lambda}$ is an energy dispersion of phonons. In the present study, we calculate $\omega_{\boldsymbol{q}\lambda}$ and $\mathrm{g}_\lambda^{m\boldsymbol{k},m'\boldsymbol{k}-\boldsymbol{q}}$ by density functional perturbation theory (DFPT) [33].

Before the electron Green's function $G_m(\boldsymbol{k}, i\omega_n)$ enters Eqs. (1) and (2), we consider the self-energy due to the electron-phonon interaction as

$$\Sigma_m(\boldsymbol{k}, i\omega_n)$$
$$= -\frac{T}{N_{\boldsymbol{k}}} \sum_{m'} \sum_{\boldsymbol{k}',i\omega_{n'}} \mathcal{K}_{mm'}^{\text{el}-\text{ph}}(\boldsymbol{k}-\boldsymbol{k}', i\omega_n - i\omega_{n'}) G_{m'}(\boldsymbol{k}', i\omega_{n'}).$$
$$(6)$$

The contribution of Coulomb interaction is not included in Eq. (6), since we usually assume that it is already contained in the Kohn-Sham energy [2]. By solving the Dyson equation self-consistently, we obtain the dressed electron Green's function

$$G_m(\boldsymbol{k}, i\omega_n) = \frac{1}{i\omega_n - \varepsilon_{m\boldsymbol{k}} - \Sigma_m(\boldsymbol{k}, i\omega_n)}, \quad (7)$$

where $\varepsilon_{m\boldsymbol{k}}$ is the bare energy dispersion of electrons. If we have *ab initio* results for $\varepsilon_{m\boldsymbol{k}}, \omega_{\boldsymbol{q}\lambda}, \mathrm{g}_\lambda^{m\boldsymbol{k},m'\boldsymbol{k}-\boldsymbol{q}}$, and $\mathcal{K}_{mm'}^{\text{C}}$, we can solve Eq. (1) and calculate T_c from first principles. It should be noted that Eq. (1) with the approximation (2) becomes an eigenvalue problem,

$$\tilde{\lambda} \Delta_m(\boldsymbol{k}, i\omega_n) = -\frac{T}{N_{\boldsymbol{k}}} \sum_{m'} \sum_{\boldsymbol{k}',i\omega_{n'}} \mathcal{K}_{mm'}(\boldsymbol{k}-\boldsymbol{k}', i\omega_n - i\omega_{n'})$$
$$\times |G_{m'}(\boldsymbol{k}', i\omega_{n'})|^2 \Delta_{m'}(\boldsymbol{k}', i\omega_{n'}). \quad (8)$$

Here we introduce a parameter $\tilde{\lambda}$ as an eigenvalue. Using the power method, we calculate $\tilde{\lambda}$ for different temperatures. The maximum eigenvalue $\tilde{\lambda}_{\max}$ reaches unity when $T = T_c$.

B. Screened Coulomb interaction

In the present study, following the SCDFT calculation [17], we employ the static approximation for the screened Coulomb interaction, which successfully reproduces the experimental T_c of elemental Nb. It should be noted that while the plasmon effect enhances T_c [34,35], spin fluctuations suppress T_c [19,36,37]. Thus SCDFT calculation considering these effects gives similar T_c to that of the static approximation [19].

Based on the results of DFT calculations, the polarizability function in the random phase approximation (RPA) can be written as [38]

$$\chi_{GG'}(q, i\omega_\nu)$$
$$= \frac{2}{N_k} \sum_{m,m'} \sum_k M^G_{mk+q,m'k} M^{G'*}_{mk+q,m'k} X_{mk+q,m'k}(i\omega_\nu), \quad (9)$$

with interstate scattering matrix

$$M^G_{mk+q,m'k} = \langle \psi_{mk+q} | e^{i(q+G)\cdot r} | \psi_{m'k} \rangle, \quad (10)$$

as well as

$$X_{mk+q,m'k}(i\omega_\nu) = \frac{f_{mk+q} - f_{m'k}}{i\omega_\nu + (\varepsilon_{mk+q} - \varepsilon_{m'k})}, \quad (11)$$

where ψ_{mk+q} and $\psi_{m'k}$ represent the Kohn-Sham wave function, f_{mk+q} and $f_{m'k}$ are the corresponding Fermi distribution function, and G and G' are reciprocal-lattice vectors. Then the RPA dielectric function is

$$\epsilon_{GG'}(q, i\omega_\nu) = \delta_{GG'} - \frac{4\pi}{\Omega} \frac{1}{|q+G|} \chi_{GG'}(q, i\omega_\nu) \frac{1}{|q+G'|}. \quad (12)$$

With the Fourier transformation of the dielectric function, combined with the bare Coulomb interaction, we can write the screened Coulomb interaction

$$w(r, r', i\omega_\nu) = \int_V dr'' \frac{\epsilon^{-1}(r, r'', i\omega_\nu)}{|r' - r''|}, \quad (13)$$

as well as its scattering matrix elements between two Kohn-Sham electrons as

$$W^{RPA}_{mk,m'k'}(i\omega_\nu) = \int_V dr \int_V dr' \psi^*_{mk}(r) \psi_{m'k'}(r) w(r, r', i\omega_\nu)$$
$$\times \psi^*_{m'k'}(r') \psi_{mk}(r'). \quad (14)$$

Therefore, we can write the Coulomb kernel in Eq. (3) as the static mode of the RPA screened Coulomb interaction:

$$\mathcal{K}^C_{mm'}(q, i\omega_\nu) = W^{RPA}_{mm'}(q, i\omega_\nu = 0), \quad (15)$$

where $q = k - k'$, and we have neglected the plasmon effect, namely the Matsubara frequency dependence of the screened Coulomb interactions. Taking average of $W^{RPA}_{mk,m'k'}(i\omega_\nu = 0)$ over the Fermi surface, we will get a parameter μ_C [39] to estimate the effect of screened Coulomb interaction of the system as

$$\mu_C N(0) = \sum_{mk,m'k'} W^{RPA}_{mk,m'k'}(i\omega_\nu = 0) \delta(\varepsilon_{mk}) \delta(\varepsilon_{m'k'}), \quad (16)$$

where $N(0)$ is the total density of states at the Fermi level.

C. Fourier transformation with the IR basis

When we solve Eqs. (6) and (8), we have to calculate the convolution of $\mathcal{K}^{el-ph}_{mm'}$ and $G_{m'}$ and that of $\mathcal{K}_{mm'}$ and $|G_{m'}|^2 \Delta_{m'}$, respectively. In general, we can write the convolution of two functions f and g on the discrete imaginary frequency grid $\{i\omega_n\}$ as

$$\sum_{i\omega_{n'}} f(i\omega_n - i\omega_{n'}) g(i\omega_{n'}) = \mathcal{F}^{-1}[\mathcal{F}(f) * \mathcal{F}(g)], \quad (17)$$

where $\mathcal{F}$ and $\mathcal{F}^{-1}$ are the Fourier and inverse Fourier transform between the imaginary frequency space $\{i\omega_n\}$ and the imaginary time space $\{\tau_m\}$, and the star $(*)$ denotes the elementwise product of two arrays. The convolution on the discrete k mesh can be calculated similarly. In the conventional calculation of T_c [12,13], we calculate Eq. (17) using the fast Fourier transformation (FFT) [40].

However, for systems with relatively low $T_c \lesssim 10$ K, the conventional FFT method will always be problematic due to its high computational cost. This is because the uniform Matsubara frequency grid of $\{i\omega_n\}$ becomes denser and denser at low temperature, while the cutoff frequency is always as high as the bandwidth $W \gtrsim 10$ eV. Thus we need to introduce a huge number of Matsubara frequencies to perform a calculation for $T \sim 10$ K.

To overcome this problem, in the present study we introduce an alternative route combining the FFT and the IR basis [24–28]. With the precomputed IR basis functions $\{U^\alpha_l\}$ [27], we have a compact and efficient representation of the Matsubara Green's function:

$$G^\alpha(i\omega_n) = \sum_{l=0}^{l_{\max}} G^\alpha_l U^\alpha_l(i\omega_n), \quad (18)$$

$$G^\alpha(\tau_m) = \sum_{l=0}^{l_{\max}} G^\alpha_l U^\alpha_l(\tau_m), \quad (19)$$

where $\alpha = $ F,B denotes the fermionic and bosonic Green's functions, respectively. The expansion of the Green's functions using the IR basis depends on two dimensionless parameters, Λ and $l_{\max}$, where $\Lambda = \beta\omega_{\max}$, $\beta = 1/T$ is an inverse temperature, and $\omega_{\max}$ is a cutoff frequency of the spectral function. The value of Λ controls the truncation errors due to the frequency window. The number of basis functions $l_{\max}$ grows only logarithmically with respect to Λ [26] (e.g., a typical value of $l_{\max}$ for $\Lambda = 10^5$ is 136, and $l_{\max}$ for $\Lambda = 10^7$ is 201). In the present study for Nb and LaH$_{10}$, we need no more than 200 IR basis functions.

We solve from Eq. (6) to (8) by means of the sparse sampling method based on the IR basis [28]. In this method, one takes sampling points in imaginary time $\{\bar{\tau}^\alpha_k\}$ $(k = 0, 1, \dots)$ according to the distribution of $l_{\max}$ roots of the highest-order basis function $U^\alpha_{l_{\max}}(\tau)$. Similarly, one takes Matsubara frequency sampling points $\{i\bar{\omega}^\alpha_k\}$ $(k = 0, 1, \dots)$ according to the distribution of the sign changes of $U^\alpha_{l_{\max}}(i\omega_n)$. This procedure always generates $l_{\max}$ or $l_{\max} + 1$ sampling points, whose distribution depends on the statistics α and Λ by construction. The sampling points are sparsely and nonuniformly distributed, covering from low- to high-frequency regions more efficiently than uniform grids.

When $i\omega_n$ is replaced by $i\bar{\omega}_k^{\alpha}$ in Eq. (18), $U_l^{\alpha}(\{i\bar{\omega}_k^{\alpha}\})$ can be regarded as a matrix element with the dimension index l and the sampling point index k. Thus, one can evaluate the expansion coefficients G_l^{α} from $G^{\alpha}(i\omega_n)$ given on the sampling points by a least-squares fitting procedure with a precomputed (pseudo) inverse of the fitting matrix. This procedure is numerically stable because the sampling points are chosen so as to minimize the condition number of the fitting matrix. The inverse transform from the right-hand side to the left-hand side is a simple matrix multiplication.

These two transforms together with their counterparts for the τ sampling enable efficient transforms between the imaginary-time and Matsubara-frequency space via the IR basis. They are much more efficient than the conventional FFT method. For example, in Sec. III A we will demonstrate that in the calculation of Nb with $T_c \sim 10$ K, the size of the fitting matrix is around 150×150 with $\Lambda = 10^5$, while the FFT requires at least 4000 Matsubara frequencies to give comparable results. We refer the reader to Ref. [28] for more technical details on the sparse sampling method.

D. Calculation conditions

In this paper, we calculate T_c of elemental Nb and LaH$_{10}$. Elemental Nb has the body-centered-cubic lattice. The lattice parameter is optimized as $a = 3.31$ Å, where the experimental value is $a = 3.30$ Å. Following Ref. [13], we take the crystal structure of the $Fm\bar{3}m$ face-centered-cubic phase of LaH$_{10}$ at 250 GPa with lattice constant $a = 4.84$ Å. For the DFT calculation, we use the QUANTUM ESPRESSO code [41] with the exchange correlation functional proposed by Perdew, Burke, and Ernzerhof [42]. We use a projector-augmented wave (PAW) [43] pseudopotential for Nb and ultrasoft pseudopotentials [44] for La and H atoms. All these pseudopotentials are provided in PSLibrary [45]. The cutoff energy for the plane-wave expansion of the wave functions is set to be 70 Ry for Nb and 50 Ry for LaH$_{10}$. The cutoffs for the charge density are 280 Ry for Nb and 500 Ry for LaH$_{10}$. For the DFPT calculation, we use the package in QUANTUM ESPRESSO [41]. For Nb, we take a $20 \times 20 \times 20$ and $18 \times 18 \times 18$ k-mesh for a $10 \times 10 \times 10$ and $9 \times 9 \times 9$ q-mesh, respectively. For LaH$_{10}$, we use a $12 \times 12 \times 12$ k-mesh and a $6 \times 6 \times 6$ q-mesh.

In the calculation of Eqs. (6) and (8), we use the conventional FFT to take a convolution on the k-mesh, and we use the IR-basis to take a convolution on the Matsubara frequency grid. For Nb, we use the number of k-points ranging from $36 \times 36 \times 36$ to $100 \times 100 \times 100$ for sampling in the first Brillouin zone to check the convergence. We use a $36 \times 36 \times 36$ k-mesh for LaH$_{10}$.

For the calculation of the screened Coulomb interaction for Nb, we use a $18 \times 18 \times 18$ and $20 \times 20 \times 20$ k-mesh for a $9 \times 9 \times 9$ and $10 \times 10 \times 10$ q-mesh, respectively. Twenty unoccupied bands are used for Nb. For LaH$_{10}$, we use a $12 \times 12 \times 12$ k-mesh, a $6 \times 6 \times 6$ q-mesh, and 30 unoccupied bands. The cutoff energy for the dielectric function is set to be 70 Ry for Nb and 50 Ry for LaH$_{10}$. The resulting Coulomb parameter in Eq. (16) is 0.24 for LaH$_{10}$ and 0.43 for Nb. In the following calculations, we use $W_{mm'}^{\text{RPA}}(\boldsymbol{q}, i\omega_\nu = 0)$ as the screened Coulomb kernel. For computing IR basis functions and the sampling points, we use the IRBASIS library [27].
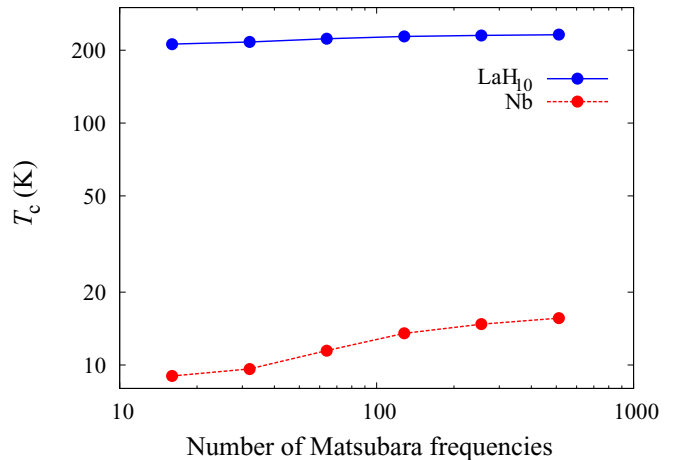

FIG. 1. N_{M} (number of Matsubara frequencies) dependence of T_c for Nb and LaH$_{10}$ at 250 GPa. Results are shown in a logarithmic scale. T_c for Nb is calculated using a $9 \times 9 \times 9$ $\boldsymbol{q}$-mesh and a $36 \times 36 \times 36$ $\boldsymbol{k}$-mesh. Data points are connected by lines.

III. RESULT AND DISCUSSION

A. Convergence along Matsubara frequencies

To solve the Eliashberg equation based on the Matsubara Green's functions, a large N_{M} has to be employed in the calculation, which causes numerical difficulty due to the expensive memory and computational time. Since the Matsubara frequencies are proportional to T, the required number of N_{M} increases linearly with decreasing T. Thus, it is extremely difficult to solve the equation in a system with low T_c. In this section, we will demonstrate this problem by comparing calculations of Nb and LaH$_{10}$ at 250 GPa, one with T_c about 10 K and the other with a high T_c around 230 K.

Figure 1 shows the numerical convergence of T_c for Nb as well as LaH$_{10}$, calculated with different numbers of N_{M}. Since LaH$_{10}$ has a high $T_c \sim 230$ K, the whole range of energy bands is covered with only several hundred Matsubara frequencies, therefore the result of T_c reaches convergence. However, with the same number of Matsubara frequencies, we cannot get a converged result of T_c for Nb, because T_c for Nb is much lower.

In Fig. 2, we compare the convergence of $\tilde{\lambda}_{\text{max}}$ for Nb and that for LaH$_{10}$ at 250 GPa (left panel), and we also show the results for Nb based on the IR basis method (right panel). For LaH$_{10}$, only a few hundred Matsubara frequencies are enough to obtain the converged value because T is sufficiently high (271.6 K). On the other hand, for Nb we need at least 4096 Matsubara frequencies to reach convergence, which is due to the low temperature used in the calculation (19.7 K). However, as is seen in the right panel of Fig. 2, $\tilde{\lambda}_{\text{max}}$ of the IR basis method reaches convergence at $\Lambda = 10^4$, which only requires $l_{\text{max}} = 103$ basis functions. Thus, it is obvious that the IR basis method performs better in Nb. Note that the IR basis method gives the same $\tilde{\lambda}_{\text{max}}$ as the conventional method in the limit of large N_{M}. In addition, comparing the computational time for a single calculation of convolution, the IR basis method with $\Lambda = 10^5$ performs 20 times faster than the conventional FFT method with 4096 Matsubara frequencies. In the follow-
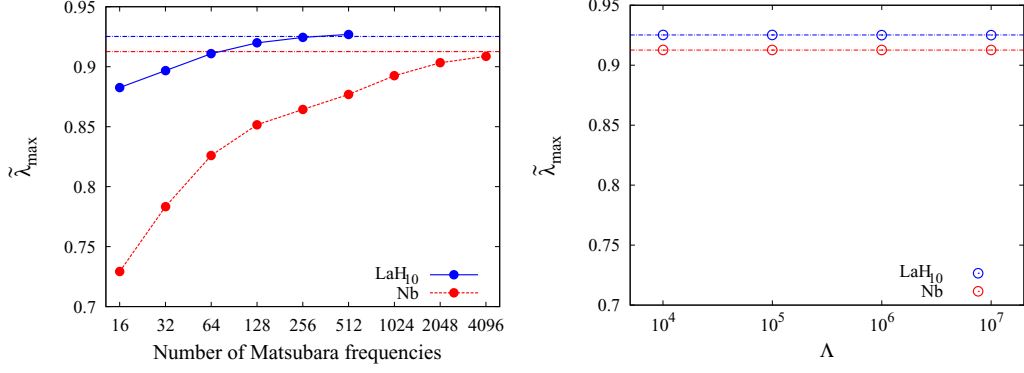
FIG. 2. Left panel: Eigenvalue $\tilde{\lambda}_{max}$ vs number of Matsubara frequencies (N_M) for Nb and LaH$_{10}$ at 250 GPa. Based on the conventional FFT method, the eigenvalue is calculated with T fixed at 19.7 K for Nb, and 271.6 K for LaH$_{10}$. The eigenvalue reaches numerical convergence with $N_M = 512$ for LaH$_{10}$, while it requires $N_M = 4096$ for Nb. Data points are connected by lines. Right panel: eigenvalue $\tilde{\lambda}_{max}$ vs dimensionless parameter Λ for Nb and LaH$_{10}$ in the IR basis method. Temperature T is fixed at 19.7 K for Nb and 271.6 K for LaH$_{10}$. The horizontal dash-dotted lines in both panels indicate that the IR basis method gives $\tilde{\lambda}_{max} = 0.913$ for Nb and $\tilde{\lambda}_{max} = 0.925$ for LaH$_{10}$, which is consistent with the converged value of $\tilde{\lambda}_{max}$ for $N_M \to \infty$. Calculations for Nb in both panels are calculated using a $9 \times 9 \times 9$ q-mesh and a $36 \times 36 \times 36$ k-mesh, and the results for LaH$_{10}$ in both panels are calculated using a $6 \times 6 \times 6$ q-mesh and a $36 \times 36 \times 36$ k-mesh.

ing calculations we set $\Lambda = 10^5$, where $l_{max} = 136$ and the number of sampling Matsubara frequency points for fermions is 138.

B. Critical temperature and gap function

In addition to the convergence test for N_M, we should also consider the convergence on a discrete k-mesh. Numerical results of different q-meshes and k-meshes are shown in Fig. 3. With the eigenvalue $\tilde{\lambda}$ in Eq. (1), we can solve
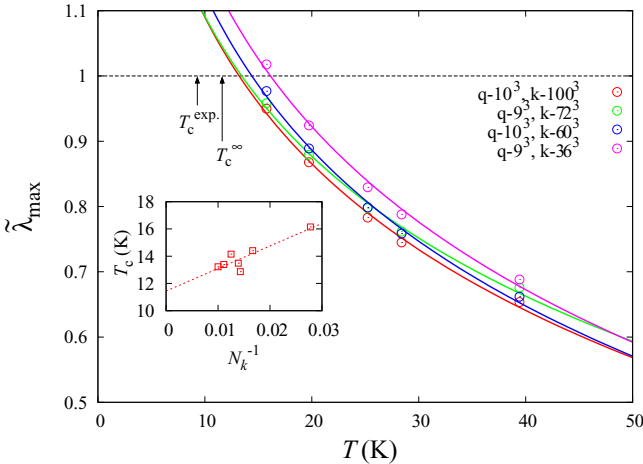

FIG. 3. Eigenvalue $\tilde{\lambda}_{max}$ vs temperature T for Nb. Circles with different colors are the results of different meshes with different numbers of sampling k points and q points. Solid lines with corresponding colors are fitting results using a fitting function $\tilde{\lambda}_{max} = A + B \ln T$. The crossing points of the fitting lines and horizontal dashed line $\tilde{\lambda}_{max} = 1$ are T_c. The numerical result of T_c for a $100 \times 100 \times 100$ k-mesh is 13.2 K. The inset shows N_k^{-1} dependence of T_c, as well as a linear fitting function $T_c = T_c^\infty + a N_k^{-1}$ as a guide to the eye, where N_k is the number of k points in one dimension. The extrapolation result of T_c with $N_k \to \infty$ is $T_c^\infty = 11.4$ K. The experimental result of T_c for Nb is $T_c^{exp.} = 9.3$ K [46].

the equation at different temperature. Then we can get a numerical result of T_c, as shown in Fig. 3. All the results of T_c with different numbers of sampling k points are shown in the inset of Fig. 3. For the calculation with a $36 \times 36 \times 36$ and $72 \times 72 \times 72$ k-mesh, a $9 \times 9 \times 9$ q-mesh is used to calculate the screened Coulomb interaction. In the calculation on the other k-meshes, the screened Coulomb interaction is calculated using a $10 \times 10 \times 10$ q-mesh. Linear interpolation is employed to use the screened Coulomb interaction data on the coarse q-mesh in the Eliashberg calculation on the dense k-mesh. T_c for a $100 \times 100 \times 100$ k-mesh is 13.2 K. The deviation between the results with different k-mesh calculations increases upon lowering the temperature since the discrete k-mesh approximation becomes less accurate. We can expect that the numerical result will become closer to the experimental value with a much denser k-mesh. A linear extrapolation of the results to the infinite number of sampling k points gives $T_c^\infty = 11.4$ K. Although this value is just a reference, it is consistent with the experimental result of $T_c^{exp.} = 9.3$ K [46].

Although we have neglected the dynamical structure of the screened Coulomb kernel, our numerical result turns out to have good agreement with the experimental T_c, which might be because we have neglected both the plasmon effects and spin fluctuations. Since the plasmon effects increase T_c and spin fluctuations decrease T_c, these two effects on T_c might counteract each other eventually. Calculations including spin fluctuations together with a dynamical Coulomb kernel [19] will be addressed in future work. We note that the value of T_c in Ref. [17] is slightly lower than that of the present study. This might be ascribed to the fact that the mass enhancement in the SCDFT is not calculated self-consistently.

In Fig. 4, we plot the normalized eigenfunction Δ of the Eliashberg equation (8) at k close to the Fermi level as a function of the Matsubara frequency. $\Delta(i\omega_n)$ changes rapidly in the range of 10^{-2}–10^{-1} eV, which is a typical energy scale of the Debye frequency. This means that the behavior of $\Delta(i\omega_n)$ in this scale is dominated by the electron-phonon
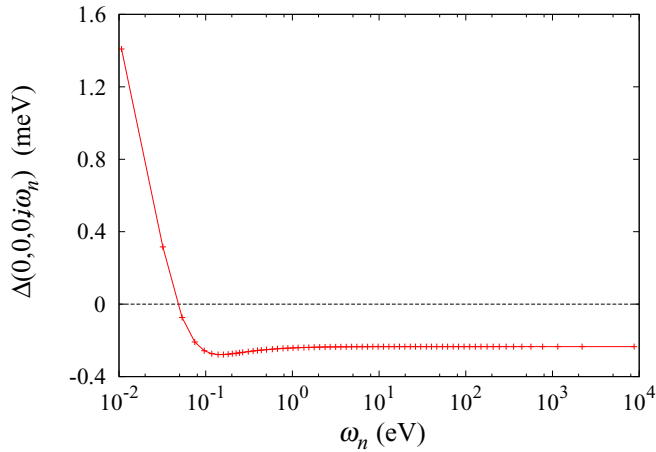
FIG. 4. Normalized eigenfunction Δ in the Eliashberg equation for Nb as a function of Matsubara frequency ω_n. Frequency sampling points are sparsely distributed along the frequency axis. Temperature is set to 39.4 K, and we use a $100 \times 100 \times 100$ $\boldsymbol{k}$-mesh. The wave number is fixed at the Γ point (0,0,0) in the Brillouin zone, and we choose the band just above the Fermi level. Data points are connected by lines.

interaction. $\Delta(i\omega_n)$ becomes negative for $\omega_n \gtrsim 10^{-1}$ eV due to the retardation effect. It should be noted that the sampling frequency points in Fig. 4 are sparsely sampled along the imaginary frequency axis. This confirms our discussions in Sec. II C that our scheme based on the IR basis can easily reach the high-energy region ~ 10 eV without introducing a huge number of Matsubara frequencies [47].

IV. CONCLUSION

We have formulated a fully *ab initio* scheme to perform calculations on the superconducting transition temperature $T_{\rm c}$, combined with the recently proposed intermediate-representation basis of the Green's function. With consideration of the fully dressed Green's function, our numerical result reproduced the experimental result without a considerably large memory and computation time cost, which is always troublesome in the conventional approach. It provides an efficient and promising approach to calculate and predict properties of superconducting systems at $T \lesssim 10$ K.

ACKNOWLEDGMENTS

APPENDIX: *K*-DEPENDENCE OF THE ELECTRON-PHONON INTERACTION MATRIX ELEMENTS

In our calculation we have used an averaged electron-phonon interaction kernel $\mathcal{K}^{\rm el-ph}_{mm'}(\boldsymbol{q}, i\omega_\nu)$, where the averaged

matrix element is written as

$$\left| g^{mm'}_\lambda(\boldsymbol{q}) \right|^2 = \frac{\sum_{\boldsymbol{k}} \left| g^{m\boldsymbol{k}, m'\boldsymbol{k}-\boldsymbol{q}}_\lambda(\boldsymbol{q}) \right|^2 \delta(\varepsilon_{m\boldsymbol{k}}) \delta(\varepsilon_{m'\boldsymbol{k}-\boldsymbol{q}})}{\sum_{\boldsymbol{k}} \delta(\varepsilon_{m\boldsymbol{k}}) \delta(\varepsilon_{m'\boldsymbol{k}-\boldsymbol{q}})}. \quad \text{(A1)}$$

When the bands m and m' are away from the Fermi level and $\left| g^{mm'}_\lambda(\boldsymbol{q}) \right|^2$ in Eq. (A1) is smaller than a threshold value, then the averaged matrix element is approximated as

$$\left| g^{mm'}_\lambda(\boldsymbol{q}) \right|^2 = \frac{1}{N_{\boldsymbol{k}}} \sum_{\boldsymbol{k}} \left| g^{m\boldsymbol{k}, m'\boldsymbol{k}-\boldsymbol{q}}_\lambda(\boldsymbol{q}) \right|^2. \quad \text{(A2)}$$

We calculate here the Eliashberg spectral function, and we examine if the $\boldsymbol{k}$-average approximation in Eqs. (A1) and (A2) is a good approximation for our calculation. We first calculate the Eliashberg function using QUANTUM ESPRESSO code, in which the Eliashberg function is defined as

$$\alpha^2 F(\omega)$$
$$= \frac{1}{N(0)} \sum_{m\boldsymbol{k}, m'\boldsymbol{k}'} \sum_\lambda \left| g^{m\boldsymbol{k}, m'\boldsymbol{k}'}_\lambda \right|^2 \delta(\varepsilon_{m\boldsymbol{k}}) \delta(\varepsilon_{m'\boldsymbol{k}'}) \delta(\omega - \omega_{\boldsymbol{q}, \lambda}),$$
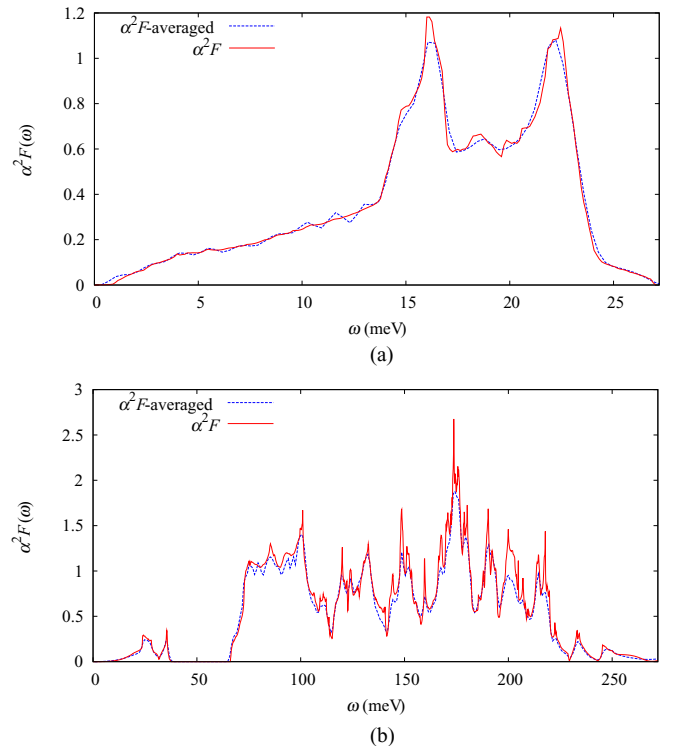$$\text{(A3)}$$

FIG. 5. (a) Eliashberg function for Nb. (b) Eliashberg function for LaH$_{10}$ at 250 GPa. The red lines are results given by $\boldsymbol{k}$-dependent matrix elements using the QUANTUM ESPRESSO code, and the blue dashed lines are results given by $\boldsymbol{k}$-averaged matrix elements using our Migdal Eliashberg calculations. The broadening of the δ-function is set to be 0.01 Ry for both $\boldsymbol{k}$-average and $\boldsymbol{k}$-dependent cases. Results for Nb are calculated using a $9 \times 9 \times 9$ $\boldsymbol{q}$-mesh and a $36 \times 36 \times 36$ $\boldsymbol{k}$-mesh, and results for LaH$_{10}$ at 250 GPa are calculated using a $6 \times 6 \times 6$ $\boldsymbol{q}$-mesh and a $36 \times 36 \times 36$ $\boldsymbol{k}$-mesh.

and $\boldsymbol{q} = \boldsymbol{k} - \boldsymbol{k}'$. Then we used the $\boldsymbol{k}$-averaged electron-phonon coupling matrix elements $|g_{\lambda}^{mm'}(\boldsymbol{q})|^2$, which are used in our Migdal-Eliashberg calculations, to replace the $\boldsymbol{k}$-dependent matrix elements $|g_{\lambda}^{mk,m'k'}|^2$ in Eq. (A3), and we calculate the corresponding $\alpha^2 F(\omega)$; then we compare the results of two Eliashberg functions.

As is shown in Fig. 5, the results of two Eliashberg functions prove that our $\boldsymbol{k}$-averaged coupling matrix elements $|g_{\lambda}^{mm'}(\boldsymbol{q})|^2$ are a good description of the electron-phonon coupling properties in these two typical phonon-mediated superconductors, which agrees with our discussion of Eq. (4) in Sec. II.

[1] P. B. Allen and B. Mitrovi, *Theory of Superconducting T_c*, edited by F. S. Henry Ehrenreich and D. Turnbull, Solid State Physics Vol. 37 (Academic Press, New York, 1983), pp. 1–92.

[2] J. A. Flores-Livas, L. Boeri, A. Sanna, G. Profeta, R. Arita, and M. Eremets, A perspective on conventional high-temperature superconductors at high pressure: Methods and materials, Phys. Rep. **856**, 1 (2020).

[3] W. L. McMillan, Transition temperature of strong-coupled superconductors, Phys. Rev. **167**, 331 (1968).

[4] P. B. Allen and R. C. Dynes, Transition temperature of strong-coupled superconductors reanalyzed, Phys. Rev. B **12**, 905 (1975).

[5] P. Morel and P. W. Anderson, Calculation of the superconducting state parameters with retarded electron-phonon interaction, Phys. Rev. **125**, 1263 (1962).

[6] F. Marsiglio, Eliashberg theory of superconductivity with repulsive coulomb enhancement, Physica C **160**, 305 (1989).

[7] F. Marsiglio, Eliashberg theory: A short review, Ann. Phys. **417** 168102 (2020).

[8] K.-H. Lee, K.-J. Chang, and M. L. Cohen, First-principles calculations of the Coulomb pseudopotential μ^*: Application to Al, Phys. Rev. B **52**, 1425 (1995).

[9] J. Carbotte, Properties of boson-exchange superconductors, Rev. Mod. Phys. **62**, 1027 (1990).

[10] F. Giustino, M. L. Cohen, and S. G. Louie, Small phonon contribution to the photoemission kink in the copper oxide superconductors, Nature (London) **452**, 975 (2008).

[11] F. Giustino, Electron-phonon interactions from first principles, Rev. Mod. Phys. **89**, 015003 (2017).

[12] W. Sano, T. Koretsune, T. Tadano, R. Akashi, and R. Arita, Effect of van Hove singularities on high-T_c superconductivity in h$_3$S, Phys. Rev. B **93**, 094525 (2016).

[13] I. Errea, F. Belli, L. Monacelli, A. Sanna, T. Koretsune, T. Tadano, R. Bianco, M. Calandra, R. Arita, F. Mauri, and J. Flores-Livas, Quantum crystal structure in the 250-kelvin superconducting lanthanum hydride, Nature (London) **578**, 66 (2020).

[14] L. N. Oliveira, E. K. U. Gross, and W. Kohn, Density-Functional Theory for Superconductors, Phys. Rev. Lett. **60**, 2430 (1988).

[15] T. Kreibich and E. K. U. Gross, Multicomponent Density-Functional Theory for Electrons and Nuclei, Phys. Rev. Lett. **86**, 2984 (2001).

[16] M. Lüders, M. A. L. Marques, N. N. Lathiotakis, A. Floris, G. Profeta, L. Fast, A. Continenza, S. Massidda, and E. K. U. Gross, *Ab initio* theory of superconductivity. i. density functional formalism and approximate functionals, Phys. Rev. B **72**, 024545 (2005).

[17] M. A. L. Marques, M. Lüders, N. N. Lathiotakis, G. Profeta, A. Floris, L. Fast, A. Continenza, E. K. U. Gross, and S. Massidda,

Ab initio theory of superconductivity. ii. application to elemental metals, Phys. Rev. B **72**, 024546 (2005).

[18] A. Sanna, *The Physics of Correlated Insulators, Metals, and Superconductors* (Verlag Forschungszentrum Jülich, Jülich, 2017), Chap. 16, p. 429.

[19] M. Kawamura, Y. Hizume, and T. Ozaki, Benchmark of density functional theory for superconductors in elemental materials, Phys. Rev. B **101**, 134511 (2020).

[20] R. Akashi, M. Kawamura, S. Tsuneyuki, Y. Nomura, and R. Arita, First-principles study of the pressure and crystal-structure dependences of the superconducting transition temperature in compressed sulfur hydrides, Phys. Rev. B **91**, 224513 (2015).

[21] J. Flores-Livas, A. Sanna, and E. K. U. Gross, High temperature superconductivity in sulfur and selenium hydrides at high pressure, Eur. Phys. J. B **89**, 63 (2016).

[22] R. Arita, T. Koretsune, S. Sakai, R. Akashi, Y. Nomura, and W. Sano, Nonempirical calculation of superconducting transition temperatures in light-element superconductors, Adv. Mater. **29**, 1602421 (2017).

[23] A. Sanna, C. Pellegrini, and E. K. U. Gross, Combining Eliashberg Theory with Density Functional Theory for the Accurate Prediction of Superconducting Transition Temperatures and Gap Functions, Phys. Rev. Lett. **125**, 057001 (2020).

[24] J. Otsuki, M. Ohzeki, H. Shinaoka, and K. Yoshimi, Sparse modeling in quantum many-body problems, J. Phys. Soc. Jpn. **89**, 012001 (2020).

[25] H. Shinaoka, J. Otsuki, M. Ohzeki, and K. Yoshimi, Compressing Green's function using intermediate representation between imaginary-time and real-frequency domains, Phys. Rev. B **96**, 035147 (2017).

[26] N. Chikano, J. Otsuki, and H. Shinaoka, Performance analysis of a physically constructed orthogonal representation of imaginary-time Green's function, Phys. Rev. B **98**, 035104 (2018).

[27] N. Chikano, K. Yoshimi, J. Otsuki, and H. Shinaoka, ir-basis: Open-source database and software for intermediate-representation basis functions of imaginary-time green's function, Comput. Phys. Commun. **240**, 181 (2019).

[28] J. Li, M. Wallerberger, N. Chikano, C.-N. Yeh, E. Gull, and H. Shinaoka, Sparse sampling approach to efficient ab initio calculations at finite temperature, Phys. Rev. B **101**, 035144 (2020).

[29] C.-H. Pao and N. E. Bickers, Renormalization-group acceleration of self-consistent field solutions: Two-dimensional Hubbard model, Phys. Rev. B **49**, 1586 (1994).

[30] F. Schrodi, A. Aperis, and P. M. Oppeneer, Increased performance of Matsubara space calculations: A case study within Eliashberg theory, Phys. Rev. B **99**, 184508 (2019).

[31] A. Migdal, Interaction between electrons and lattice vibrations in a normal metal, Sov. Phys. JETP **34**, 996 (1958).

[32] G. Eliashberg, Interactions between electrons and lattice vibrations in a superconductor, Sov. Phys. JETP **11**, 696 (1960).

[33] S. Baroni, S. de Gironcoli, A. Dal Corso, and P. Giannozzi, Phonons and related crystal properties from density-functional perturbation theory, Rev. Mod. Phys. **73**, 515 (2001).

[34] R. Akashi and R. Arita, Development of Density-Functional Theory for a Plasmon-Assisted Superconducting State: Application to Lithium Under High Pressures, Phys. Rev. Lett. **111**, 057006 (2013).

[35] R. Akashi and R. Arita, Density functional theory for plasmon-assisted superconductivity, J. Phys. Soc. Jpn. **83**, 061016 (2014).

[36] F. Essenberger, A. Sanna, A. Linscheid, F. Tandetzky, G. Profeta, P. Cudazzo, and E. K. U. Gross, Superconducting pairing mediated by spin fluctuations from first principles, Phys. Rev. B **90**, 214504 (2014).

[37] F. Essenberger, A. Sanna, P. Buczek, A. Ernst, L. Sandratskii, and E. K. U. Gross, Ab initio, Phys. Rev. B **94**, 014503 (2016).

[38] W. G. Aulbur, L. Jönsson, and J. W. Wilkins, Quasiparticle calculations in solids, Solid State Physics **54**, 1 (2000).

[39] It should be noted that using the quantities we have obtained, it is possible to perform the Morel-Anderson renormalization such as μ^* evaluation [8]. In our approach, however, we directly use W^{RPA} instead of μ_C or μ^*. Our scheme of solving Eqs. (1) and (8) directly is more straightforward, compared to conventional Eliashberg calculations with μ^* involved.

[40] M. Frigo and S. G. Johnson, The design and implementation of FFTW3, Proc. IEEE **93**, 216 (2005), special issue on "Program Generation, Optimization, and Platform Adaptation".

[41] P. Giannozzi, O. Andreussi, T. Brumme, O. Bunau, M. B. Nardelli, M. Calandra, R. Car, C. Cavazzoni, D. Ceresoli, M. Cococcioni, N. Colonna, I. Carnimeo, A. D. Corso, S. de Gironcoli, P. Delugas, R. A. DiStasio Jr., A. Ferretti, A. Floris, G. Fratesi, G. Fugallo, R. Gebauer, U. Gerstmann, F. Giustino, T. Gorni, J. Jia, M. Kawamura, H.-Y. Ko, A. Kokalj, E. Küçükbenli, M. Lazzeri, M. Marsili, N. Marzari, F. Mauri, N. L. Nguyen, H.-V. Nguyen, A. O. de-la Roza, L. Paulatto, S. Poncé, D. Rocca, R. Sabatini, B. Santra, M. Schlipf, A. P. Seitsonen, A. Smogunov, I. Timrov, T. Thonhauser, P. Umari, N. Vast, X. Wu, and S. Baroni, Advanced capabilities for materials modeling with QUANTUM ESPRESSO, J. Phys.: Condens. Matter **29**, 465901 (2017).

[42] J. P. Perdew, K. Burke, and M. Ernzerhof, Generalized Gradient Approximation Made Simple, Phys. Rev. Lett. **77**, 3865 (1996).

[43] P. E. Blöchl, Projector augmented-wave method, Phys. Rev. B **50**, 17953 (1994).

[44] D. Vanderbilt, Soft self-consistent pseudopotentials in a generalized eigenvalue formalism, Phys. Rev. B **41**, 7892 (1990).

[45] A. Dal Corso, Pseudopotentials periodic table: From H to Pu, Comput. Mater. Sci. **95**, 337 (2014).

[46] N. Ashcroft and N. Mermin, *Solid State Physics* (Cornell University Press, Ithaca, NY, 1976).

[47] We note that the gap function is a constant over a large range of Matsubara frequencies. Though it is possible to perform the Morel-Anderson renormalization for the gap function, we have not pursued that treatment in this work.